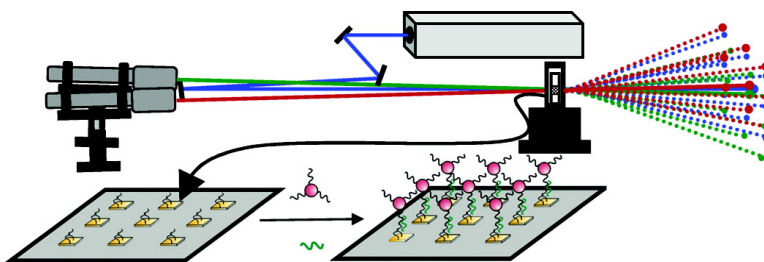Article

Real-Time Multicolor DNA Detection with Chemoresponsive Diffraction Gratings and Nanoparticle Probes

Ryan C. Bailey, Jwa-Min Nam, Chad A. Mirkin, and Joseph T. Hupp

More About This Article

Additional resources and features associated with this article are available within the HTML version:

- Supporting Information
- Links to the 17 articles that cite this article, as of the time of this article download
- Access to high resolution figures
- Links to articles and content related to this article
- Copyright permission to reproduce figures and/or text from this article

View the Full Text HTML

Real-Time Multicolor DNA Detection with Chemoresponsive Diffraction Gratings and Nanoparticle Probes

Ryan C. Bailey, Jwa-Min Nam, Chad A. Mirkin,* and Joseph T. Hupp*

Contribution from the Department of Chemistry and Institute for Nanotechnology, Northwestern University, Evanston, Illinois 60208

Received April 5, 2003; E-mail: jthupp@chem.northwestern.edu; camirkin@chem.northwestern.edu

Abstract: We report a real-time DNA detection method that utilizes single-strand DNA-modified nanoparticle probes and micropatterned chemoresponsive diffraction gratings interrogated simultaneously at multiple laser wavelengths. The surface-bound nanoparticle probe based assay with the chemoresponsive diffraction grating signal transduction scheme results in an experimentally simple DNA detection protocol, displaying attributes of both detection methodologies: the high sensitivity and selectivity afforded by nanoparticle probes and the experimental simplicity, wavelength-dependent resonant enhancement features, and miniaturization potential provided by the diffraction-based sensing technology.

Introduction

In this report, we present a real-time DNA detection methodology that utilizes single-strand (ss) DNA-modified nanoparticle probes and micropatterned chemoresponsive diffraction gratings simultaneously interrogated at multiple wavelengths. Oligonucleotide-modified nanoparticle assays have been reported that rely upon a red-to-blue color change accompanying target hybridization with unusual sensitivity and selectivity in detecting target DNA strands and proteins.[1–7] This color change, observed with a UV−vis spectrometer, is caused by the change in dielectric environment that accompanies the formation of a DNA−gold nanoparticle network aggregate in solution.

Recently, a new chemical sensor transduction mechanism was introduced that is sensitive to changes in the local dielectric environment[8] within a micropatterned chemoresponsive diffraction grating.[9–12] For example, displacement of water by a higher dielectric molecular analyte on the grating surface or within a porous grating material results in an easily observable increase in grating diffraction efficiency.[13] The response obviously can be made chemically selective by coupling analyte uptake to molecular recognition. Alternatively, and less obvious, selectivity can be engendered in the *readout* step by coupling uptake to an analyte-specific color change, either of the analyte itself or of the grating. For example, chloroform can be readout preferentially by ca. 3500-fold relative to methanol when these are taken up by a nonchemically selective grating composed of a mildly vapochromic charge-transfer salt.[9] Implied by the preferential readout is a very substantial amplification of the grating signal, although attenuation of undesired signals is also possible. The optical basis for both the amplification and selective readout is in the contribution of resonant imaginary or absorptive components of the refractive index to the observed changes in diffraction efficiency.

We reasoned that a combination of the surface-bound nanoparticle probe-based assay with the chemoresponsive diffraction grating signal transduction scheme would result in an experimentally straightforward DNA detection protocol, displaying attributes of both detection methodologies. These include the high sensitivity and selectivity afforded by nanoparticle probes, as well as the experimental simplicity, and wavelength-dependent (chromophoric probe particle dependent) resonance amplification features provided by the diffraction-based sensing technology. Significantly, this method permits real-time observation of DNA hybridization on surfaces with very good sensitivity (40−900 fM (extrapolated), depending on probe wavelength), and since no chemical enhancement process is required, the sensing platform is reusable after an appropriate dehybridization protocol. Furthermore, the grating-based methodology is, in principle, amenable to miniaturization given that only simple, inexpensive laser sources and small photodiode detectors are required for device construction.

(1) Mirkin, C. A.; Letsinger, R. L.; Mucic, R. C.; Storhoff, J. J. *Nature* **1996**, *382*, 607−609.
(2) Elghanian, R.; Storhoff, J. J.; Mucic, R. C.; Letsinger, R. L.; Mirkin, C. A. *Science* **1997**, *277*, 1078−1080.
(3) Storhoff, J. J.; Elghanian, R.; Mucic, R. C.; Mirkin, C. A.; Letsinger, R. L. *J. Am. Chem. Soc.* **1998**, *120*, 1959−1964.
(4) Taton, T. A.; Mirkin, C. A.; Letsinger, R. L. *Science* **2000**, *289*, 1757−1760.
(5) Park, S.-J.; Taton, T. A.; Mirkin, C. A. *Science* **2002**, *295*, 1503−1506.
(6) Nam, J.-M.; Park, S.-J.; Mirkin, C. A. *J. Am. Chem. Soc.* **2002**, *124*, 3820−3821.
(7) Jin, R.; Wu, G.; Li, Z.; Mirkin, C. A.; Schatz, G. C. *J. Am. Chem. Soc.* **2003**, *125*, 1643−1654.
(8) Representative of reports on other refractive index based signal-transduction schemes are the following: (a) Thiel, A. J.; Frutos, A. G.; Jordan, C. E.; Corn, R. M.; Smith, L. M. *Anal. Chem.* **1997**, *69*, 4948−4956. (b) Dancil, K.-P. S.; Greiner, D. P.; Sailor, M. J. *J. Am. Chem. Soc.* **1999**, *121*, 7925−7930. (c) Chan, S.; Horner, S. R.; Miller, B. L.; Fauchet, P. M. *J. Am. Chem. Soc.* **2001**, 123, 11797−11798. (d) Riboh, J. C.; Haes, A. J.; McFarland, A. D.; Ranjit, C.; Van Duyne, R. P. *J. Phys. Chem. B* **2003**, *107*, 1772−1780.
(9) Bailey, R. C.; Hupp, J. T. *J. Am. Chem. Soc.* **2002**, *124*, 6767−6774.
(10) Bailey, R. C.; Hupp, J. T. *Anal. Chem.* **2003**, *75*, 2392−2398.
(11) Mines, G. A.; Tzeng, B.; Stevenson, K. J.; Li, J.; Hupp, J. T. *Angew. Chem.* **2002**, *41*, 154−157.
(12) Massari, A. M.; Stevenson, K. J.; Hupp, J. T. *J. Electroanal. Chem.* **2001**, *500*, 185−191.
(13) Dang, X.; Stevenson, K. J.; Hupp, J. T. *Langmuir* **2001**, *17*, 3109−3112.

Scheme 1. Illustration of Detection Methodology
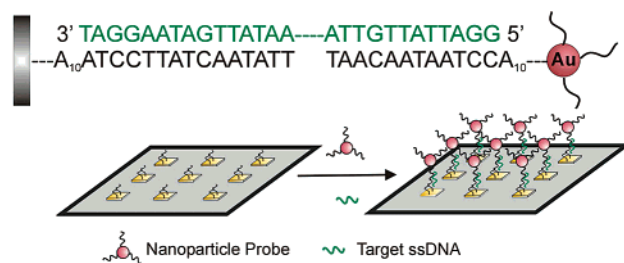
Experimental Section

The overall grating fabrication strategy includes the preparation of thin micropatterned Au gratings and subsequent functionalization with an appropriate 5′ thiolated DNA single strand (in this case, 5′ HS-A_{10}ATCCTTATCAATATT 3′). Hybridization of a solution-phase target (5′ GGATTATTGTTAAATATTGATAAGGAT 3′) leads to the localization of a complementary 3′ thiolated ssDNA-functionalized (5′ TAACAATAATCCA$_{10}$−SH 3′) 13 nm Au particles, Scheme 1. In proximity to the grating structure, the presence of the nanoparticle probe leads to measurable changes in the observed diffraction efficiency.

Probes and DNA strands were synthesized and purified by literature methods.[3,14] In a typical experiment, a 4 × 4 mm regular array of 5 × 5 μm squares was photolithographically patterned onto transparent glass microscope slides (Fisher Scientific, Pittsburgh, PA) that had been cleaned by 20 min immersion into an aggressive cleaning solution (3:1 H_2SO_4/30% H_2O_2)[15] at 60 °C, rinsed copiously with water, and blown dry in a stream of N_2. Thermal evaporation of Ti (2 nm) and Au (10 nm) followed by removal of resist via sonication in acetone resulted in the fabrication of an optically transparent diffraction grating. To minimize nonspecific DNA binding, the substrate was then passivated with a solution of 2% octadecyltrimethoxysilane (OTS) in toluene for 2 h followed by surface modification in a 2 μM 5′ SH-ssDNA solution for 24 h. An optical micrograph of a representative micropatterned grating is shown as Figure 1 (white scale bar is 10 μm).

With the grating submerged in 750 μL of 2 nM Au nanoparticle probes, 84 μL of stock target ssDNA was injected via syringe. Diffraction measurements began concurrently with the addition of the stock solution. Multiple stock concentrations were employed, yielding final target ssDNA concentrations ranging from 1 pM to 100 nM (800 attomoles to 80 picomoles).

A diagram of the experimental setup used in the diffraction measurements is shown in Scheme 2. Diffraction-based sensor measurements were made by simultaneously passing three laser beams through the grating, contained in an OTS-passivated reduced-volume cuvette held in a temperature controlled sample stage (Quantum Northwest, Spokane, WA). The lasers employed, two Helium−Neon lasers (λ = 632.8 and 543.5 nm; Melles-Griot, Carlsbad, CA) and a diode-pumped Millennia X Nd/YAG laser (λ = 532 nm; Spectra-Physics, Mountain View, CA), were spatially overlapped at the grating surface at slightly different angles of incidence.[16] The intensities of the diffracted spots ($(I_{0,0})$ and $(I_{1,0})$, subscripts reflecting diffracted order and direction) were measured by silicon photodiodes (Thorlabs, Newton, NJ), amplified as needed by home-built voltage-following op-amps and digitized by a custom LabView interface at a rate of 1 Hz. Data treatment involved ratioing the diffracted and undiffracted diode signals to obtain an operational diffraction efficiency (DE). With measurements defined in this way, losses (or changes in losses) due to reflection, scattering, absorption and so on, because they affect diffracted and undiffracted light intensities essentially equivalently, do not significantly
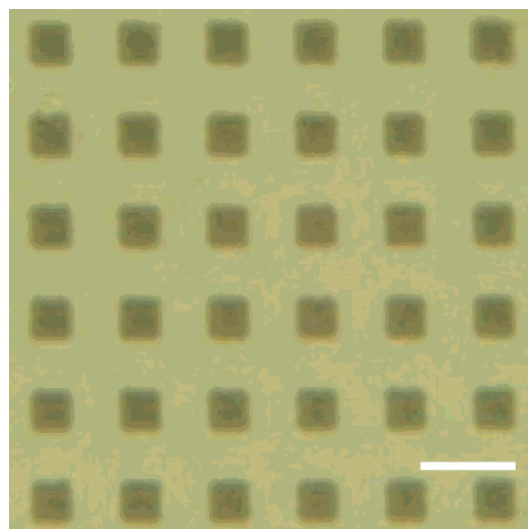
(14) Eckstein, F. *Oligonucleotides and analogues*; Oxford University Press: New York, 1991.
(15) **Caution!** Pirahna solutions are extraordinarily dangerous, reacting explosively with trace quantities of organics.
(16) In contrast to SPR measurements, small differences in angle of incidence are of little consequence for grating efficiency measurements.

Figure 1. Optical micrograph of a typical ssDNA-functionalized micropatterned gold grating used for diffraction-based hybridization measurements.

Scheme 2. Diagram of Experimental Diffraction-Based Sensing Setup
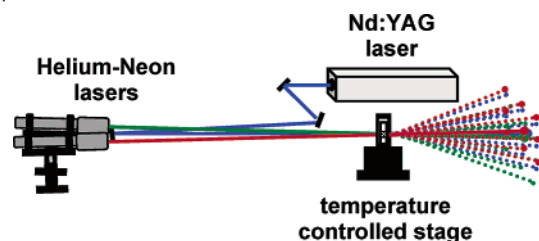
influence the final signal magnitude. The modulation in diffraction efficiency upon exposure to ssDNA was then determined by normalizing the diffraction efficiency following exposure to target (DE_{target}) to that before exposure (DE_0).

$$\Delta DE\% = \left(\frac{DE_{target} - DE_0}{DE_0}\right) \times 100\% \qquad (1)$$

Results

Figure 2 shows the time-resolved responses of two ssDNA-functionalized gratings upon exposure to target concentrations of 100 nM (Figure 2a) and 100 pM (Figure 2b). As can be seen in Figure 2, diffraction responses measured at different laser wavelengths show remarkably different patterns. In Figure 2a, the diffraction efficiencies at all three probe colors initially decrease, but the responses at both 543 and 532 nm inflect, becoming positive at longer times. In contrast, the diffraction efficiency at 633 nm continues to become more negative. In Figure 2b, however, a negative signal is observed throughout the hybridization process with all three probe colors. Figure 3a summarizes the final (long-time) responses of 5′ ssDNA-functionalized gratings to a wide range of target concentrations. Corresponding colored diamonds (Figure 3b) represent estimated detection limits (defined as 3σ for signal-to-noise) for the three probe colors. The values are 900, 40, and 750 fM (750, 33, and 625 attomoles) at probe wavelengths 633, 543, and 532 nm, respectively. They were obtained by linear extrapolation from signal magnitudes and errors observed for the 1 pM target concentration experiment. Direct assessment of the estimated 40 fM detection limit was precluded by the increasingly longer
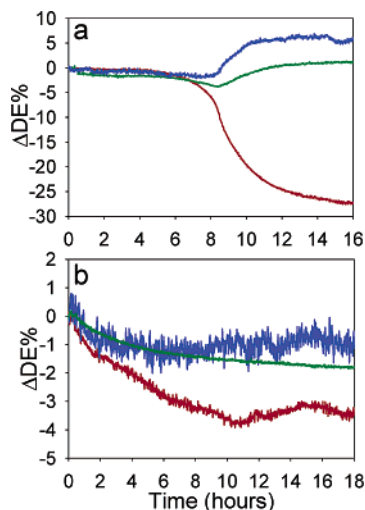
Figure 2. Real-time hybridization of target ssDNA (the anthrax lethal factor sequence; Scheme 1) and nanoparticle probes to micropatterned diffraction gratings as observed simultaneously at three different laser wavelengths. Target concentrations are (a) 100 nM and (b) 100 pM. (red = 633 nm, green = 543 nm, and blue = 532 nm).
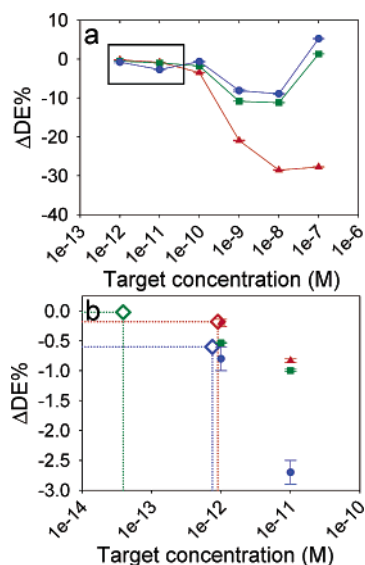

Figure 3. (a) Responses of diffraction-based detection system to varying concentrations of complementary target ssDNA. Error bars are included with each data point. (b) Expanded region (rectangle) of Figure 3a showing 1 pM and 10 pM responses (red = 633 nm, green = 543 nm, and blue = 532 nm).

times required for hybridization at lower target concentrations in the diffusionally inefficient cell employed.[17]

Corroboration of target hybridization and accompanying nanoparticle probe localization was obtained, in part, via visible-region absorption/extinction spectroscopy. The optical extinction spectra of nonpatterned ssDNA-functionalized Au films, both pre- and post-target 100 nM target ssDNA hybridization, are shown in Figure 4. Extinction spectra of films hybridized at lower target concentrations yielded much weaker nanoparticle plasmon absorptions preventing quantitative assessment. Further corroboration of interfacial hybridization and a crude estimate of its extent at 10 pM target concentration were obtained via
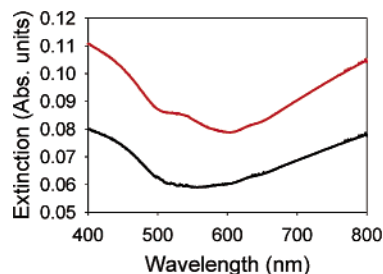
(17) Though it is clear from Figure 3a that the observed signal is highly nonlinear over the full dynamic range of the sensor, for reasons detailed in the Discussion section, the response should be linear for extrapolation in the low concentration range.

Figure 4. Visible-region extinction spectrum of an ssDNA-functionalized gold grating pre- (black line) and postexposure (red line) to 100 nM complementary target ssDNA.
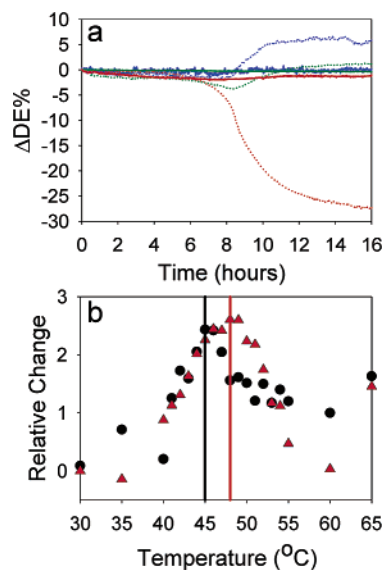

Figure 5. (a) Real-time hybridization response upon grating exposure to 100 nM concentration of noncomplementary ssDNA (red = 633 nm, green = 543 nm, and blue = 532 nm). For reference, the corresponding complementary-strand responses at 100 nM (dotted lines) have been included. (b) Temperature-dependent melting behavior of complementary (▲) and noncomplementary (●) target ssDNA as observed at 633 nm. Melting temperatures were found to be 48 °C and 45 °C, for complementary and noncomplementary strands, respectively.

tip-convoluted AFM measurements. At this concentration, but not at high concentrations, interparticle spacing is large enough to permit reasonably accurate particle counting; these measurements show roughly 25 particles in a 5×5 μm^2 area (i.e., the area of one pad for a micropatterned film).

To investigate the sequence specificity of the diffraction-based assay, the hybridization of a noncomplementary target strand (an HIV target;[18] 5′ AGAAGATATTTGGAATAACATGAC-CTGGAT 3′) was monitored. Under identical hybridization conditions, using a 633 nm probe beam, a 100 nM solution of the noncomplementary strand elicited a significantly smaller diffraction response, 25 times less than seen with the complementary strand. The full time-resolved multicolor diffraction responses of 100 nM complementary and noncomplementary target concentrations hybridized to a functionalized grating, in a solution containing complementary nanoparticle probes, are compared in Figure 5a.

Additionally, the diffraction technique was used to monitor and compare the thermal dehybridization of duplexes formed

(18) HIV-1 isolate 97ZM057F from Zambia nonfunctional envelope glycoprotein (env) gene (AF405180, b., *N166−198th*). Detailed information is available on the National Center fro Biotechnology Information (NCBI) website: http://www2.ncbi.nlm.nih.gov/Genbank/index.html.

with complementary versus noncomplementary target ssDNA. Identical gratings were exposed to 100 nM solutions of one or the other type of strand, and diffraction efficiencies were evaluated at several temperatures between 10 and 80 °C. Normalizing for initial signal magnitudes (Figure 5a), we found that increasing the cuvette temperature increases the relative diffraction efficiency to a point and then decreases (after correction for a complex background response, the origin of which we do not yet fully understand; data displayed in Figure 5b are background-corrected data). Identifying the DNA duplex melting temperature as the temperature at which the signal in Figure 5b inverts, we obtained for complementary and noncomplementary structures, respectively, values of 48 °C and 45 °C. While differing only modestly, these are consistent with previous reports.[4] At the same time, potential difficulties in the deconvolution of the temperature-dependent background grating response make the implementation of melting temperature alone unlikely to be a suitable diagnostic for complementary versus noncomplementary target DNA detection. Instead, the signal magnitude and its evolution with time (Figure 5a) should be used.

Theoretical Description

Assuming that the measured changes in diffraction efficiency are completely the result of nanoparticle capture, an expression can be written describing the observed change in diffraction efficiency as a function of only the refractive index contributions of the nanoparticle probes and the initial (prehybridization) grating index contrast at a single wavelength:[19]

$$\Delta DE\% = b \cdot \left[\frac{-n_{nanoparticles}}{\Delta n_0} \cdot 100\% \right] \qquad (2)$$

In the equation, b is a scaling constant, $n_{nanoparticles}$ is the nanoparticle refractive index contribution, and Δn_0 is the initial index contrast.

The refractive index modulation contributed by the nanoparticles can be calculated using the Kramers−Kronig expression (eq 3), which considers the effect of optical absorption, in this case the intense plasmon absorption of the nanoparticle probes, on the real component of the refractive index:[9]

$$n_{nanoparticles}(\omega') = \frac{c}{\pi} \int_0^\infty \frac{\alpha(\omega)}{\omega^2 - \omega'^2} \, d\omega \qquad (3)$$

In this equation, c is the speed of light, α is the absorptivity, and ω is the angular frequency of the incident light.[20]

It follows that if there is a change in absorptivity (in other words, a change in imaginary component of the refractive index), there will be a corresponding (via eq 3) change in the real part of the refractive index, a change in the index contrast (Δn), and, ultimately, a change in diffraction efficiency. Equations 2 and 3 further imply that the changes in diffraction efficiency, due to absorptivity effects, will be wavelength dependent. Notably, the changes in diffraction efficiency brought by absorptivity effects can be the same sign as simple real-component effects or opposite in sign. Additionally, the absorptivity effects can sometimes exceed, by multiple orders of

magnitude, the simple real component effects. Consequently, absorptivity effects can be used to obtain wavelength-dependent amplification of chemoresponsive grating signals.

Also accompanying absorptivity changes will be absorption and possibly reflection losses. Because ΔDE is operationally defined as a ratio, however, these losses do not effect the signals.

Discussion

At low target concentrations, the number of nanoparticles captured is small enough that their random distribution over the micropatterned platforms results in little electromagnetic communication between particles and causes only a small alteration of nanoparticle plasmon absorption from that observed in solution.[21] Higher target concentrations lead to an increased number of captured nanoparticles, resulting in a significant redshift and broadening of the plasmon absorption due to aggregation effects, analogous to those seen in solution-based assays.[3] We reasoned that if the diffraction response is dominated by Kramers−Kronig type resonance amplification (and deamplification) effects, then complex probe-wavelength-dependent and nanoparticle-coverage-dependent behavior would be expected and would likely explain the disparate and nonmonotonic responses encountered experimentally.

To test the idea, eqs 2 and 3 were used, where the latter requires grating-localized absorption spectra. As noted above, accurate spectra for the captured nanoparticle probes proved difficult to measure under these conditions. Consequently, spectra were simulated as Gaussian peaks with absorption maxima and line widths assigned consistent with previous experimental[22] and theoretical findings[23] for surface-bound gold nanoparticles and nanoparticle aggregates.[24] Plasmon absorption spectra for the nanoparticle probes were simulated at each of the three surface loadings chosen to be representative of increasing numbers of captured probes accompanying increasing target concentrations corresponding roughly to 1−10 pM, 100 pM−1 nM, and 100 nM. The results of this modeling are shown in Figure 6a.

With these spectra in hand, the refractive index contributions of the nanoparticles at varying target concentrations were calculated according to eq 3 and are shown as a function of wavelength in Figure 6b. Noteworthy are (a) the existence of both positive and negative contributions, depending on the wavelength, and (b) changes in the shapes of the curves, including the wavelength distribution of positive versus negative contributions, with changes in loading.

Via eq 2, changes in diffraction efficiency were calculated using the refractive index contributions of the captured nanoparticle probes (Figure 6b). Utilizing bulk refractive index values of gold[25] and the refractive index of water ($n_{water} = 1.33$) to determine Δn_0, we qualitatively modeled relative changes in

(19) According to eq 3, assuming constant grating thickness.
(20) $[\alpha = 2.3 \cdot OD(\lambda)/t]$ and $[\omega = 2\pi c/\lambda]$, where c is the speed of light, λ is the wavelength of light, $OD(\lambda)$ is the optical density of the grating, and t is the grating thickness.
(21) Mere proximity of the bound particles to the gold platform, however, should also alter the particles' plasmon absorption to a small extent. For simplicity, and because we lack quantitative information about the anticipated alteration, we neglect this effect in the discussion that follows.
(22) Bailey, R. C.; Stevenson, K. J.; Hupp, J. T. *Adv. Mater.* **2000**, *12*, 1930−1934.
(23) Kelly, K. L.; Coronado, E.; Zhao, L. L.; Schatz, G. C. *J. Phys. Chem. B* **2003**, *107*, 668−677.
(24) Experimental extinction spectra for surface and solution aggregates of gold nanoparticles generally feature significant scattering components in addition light absorption. Equation 3, on the other hand, employs only the absorption component.
(25) The real component refractive indices used were $n_{(532nm)} = 0.5571$, $n_{(544nm)} = 0.4676$, and $n_{(632nm)} = 0.1797$.
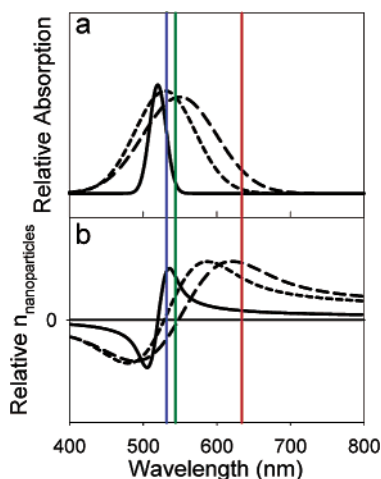
Figure 6. (a) Modeled absorption spectra from captured gold nanoparticle probes at varying target concentrations (— = 1–10 pM, - - - = 100 pM–10 nM, and – – – = 100 nM). With increasing nanoparticle loading onto the surface, the surface plasmon band characteristically red-shifts and broadens. (b) Refractive index contributions from nanoparticle absorption spectra (part a) as calculated by eq 1. For reference, the laser lines used experimentally have been outlined (red = 633 nm, green = 543 nm, and blue = 532 nm).
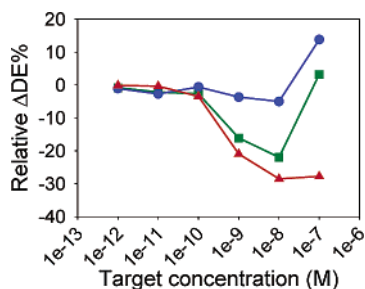

Figure 7. Calculated concentration-dependent changes in the relative diffraction efficiency upon target hybridization and nanoparticle probe capture, according to eq 2 (red = 633 nm, green = 543 nm, and blue = 532 nm).

diffraction efficiency over the experimentally investigated concentration range. In the modeling, account was taken of both changes in overall absorption intensity with changes in nanoparticles coverage and changes in spectral line shape. The results of these calculations, scaled to experimental values at 633 nm, are shown in Figure 7. Calculated and experimentally measured (Figure 3) concentration-dependent responses show markedly good agreement over the majority of the interrogated concentrations indicating, at least, the qualitative integrity of the model. In particular, the modeling accounts for both the sign reversal for ΔDE with increasing target concentration at two of the probe wavelengths and the absence of such an effect at the third wavelength.

The origin of the observed signal direction and sign reversal is the small real refractive index component of the employed gold pads over the visible region.[25] In contrast to previous reports,[9–13] the small index of the grating material, smaller than that of the surrounding environment, results in "inverse" grating contrast (for example, at $\lambda = 633$ nm, $\Delta n_0 = |n_{gold} - n_{water}| = |0.18 - 1.33| = 1.15^{26}$). Subsequent target hybridization and

nanoparticle probe localization result in a further modulation of the grating index contrast. In the case of postresonant (lower energy) probe wavelengths and particle loadings, the Kramers–Kronig contributions of the nanoparticle probes lead to a net decrease in index contrast and thus a decrease in the observed diffraction efficiency. Analogously, preresonant (higher energy) wavelengths and particle loadings (100 nM) result in an increase in grating contrast, hence an increase in diffraction efficiency.

The modeling also provides a qualitative explanation for the peculiar temporal evolution of diffraction efficiencies at a fixed solution-phase concentration of complementary target DNA (Figure 2). Briefly, as the number of captured nanoparticles increases, their contribution to the diffraction response becomes greater. From the Kramers–Kronig analysis, the contribution is positively signed (Δn, the refractive index contrast, decreases) at all probe wavelengths examined. Later, when some critical coverage or range of coverages is reached, the spectrum red-shifts and (because of the higher coverage) intensifies. These changes conspire, again via the Kramers–Kronig relation, to reverse the sign of the nanoparticles' contribution to the overall diffraction efficiency obtained at 532 and 543 nm. At 633 nm, on the other hand, the absorption spectral changes merely enhance the particles' contribution to the measured diffraction efficiency, but without changing the sign of the contribution. Finally, the simpler time dependence seen for noncomplementary DNA (the diffraction efficiency monotonically decreases at all probe wavelengths; Figure 5) is a consequence of the coverages attained. For the comparatively poorly bound non-complementary target, the critical coverage for substantive spectral shifting and accompanying Δn sign reversal evidently is not reached.

What about absorption of light by gold particles in the solution phase? Measurements were typically made in the presence of a 2 nM solution of nanoparticle probes that indeed presents significant optical density, so it might seem to be a signal obscurant. However, the experiments yield signals only for material that binds to the patterned platform (grating) and not from any unpatterned constituents (e.g., nanoparticles in solution). In other words, we are blind to absorption behavior in the solution phase.[27] One important consequence is that data can be collected in situ and in real time; a solution removal or replacement step is unnecessary. We view this as one of the more significant advantages of the new methodology.

Returning to the Kramers–Kronig modeling, implied is a significant degree of resonance enhancement. We reasoned that the degree of enhancement could be gauged by performing target capture experiments such as those described above, but without nanoparticles tags, the putative sources of enhancement. Under these conditions, the sign of the diffraction efficiency change should be the same at all wavelengths (and at all times), since the chromophoric probes, and corresponding resonance effects, are absent. Table 1 shows results obtained with a 100 nM solution of ssDNA target. In contrast to results obtained with particle-tagged capture strands, the sign of ΔDE is the same for the three probe wavelengths. Furthermore, the observed negative sign is consistent with displacement of grating-proximal water ($n = 1.33$) by organic material of higher refractive index

---

(26) The index contrast of the grating, prior to hybridization, also contains a contribution from the attached ssDNA; however, the contribution is small in an effective medium context (see ref 9), so is neglected in calculations here.

(27) Recall that DE is defined here as a ratio of diffracted-to-undiffracted light intensities; both are attenuated by solution absorption but to precisely proportional extents.

Table 1. Multicolor Diffraction Responses for Target Hybridization to 5′ Complementary Strands with and without Attached Nanoparticle Probes

	ΔDE% $\lambda = 532$ nm	ΔDE% $\lambda = 543$ nm	ΔDE% $\lambda = 633$ nm
5′ complementary strand functionalized nanoparticle probe	5.59	1.18	−27.45
5′ complementary strand without nanoparticle probe	−3.35	−2.97	−3.17

($n \approx 1.4$), thus lowering the net refractive index contrast. In the best case, utilizing nanoparticle probes as hybridization beacons, as shown in Table 1, yields a roughly 8-fold signal response amplification (measurements at 633 nm).

Evident as well (measurements at 532 and 543 nm) is resonance deamplification, reflecting the difference in sign between the simple real component contribution to ΔDE and the absorptivity-induced contribution to ΔDE. Also of interest is the approximate wavelength independence of ΔDE in the nonresonant measurements (nanoparticle-free experiments). In contrast, a greater than 20-fold difference in absolute diffraction efficiency change can be observed by altering the laser probe wavelength, a finding that has obvious implication for multiplexing as discussed briefly below. (Clearly for simple sensing experiments, however, only a single wavelength is required.)

Closely related to the issue of signal amplification is the question of detection limit. A limit of ca. 40 fM can be inferred from 633 nm measurements, admittedly extrapolated from a much higher target concentration. A potential problem with the extrapolation, especially in a much shorter pathlength (smaller volume) cell, is that the relatively large area grating may deplete the sample solution of target, yielding fewer than expected target strands per pad and a poorer than anticipated detection limit. It is important to note, however, that the grating used is massively redundant with respect to diffraction; as few as a dozen pads configured as a 1D grating will diffract nearly as well as the 160 000 pads used here. While beyond the scope of this paper, grating miniaturization using silicon supports and conventional electronic-materials-applicable lithographic techniques is a primary focus of current work. An obvious way to extend the detection limit would be to achieve a better match of the Kramers−Kronig-transformed nanoparticle plasmon band with the wavelength of the probe laser. That the existing match is less than optimal is illustrated in an interesting way by the measurements and modeling in Figures 3, 6, and 7, where lateral aggregation of particles at high target strand concentration favorably shifts the plasmon band, thereby substantially amplifying the signal.

Because the chemoresponsive grating approach to DNA detection, at least as implemented here, relies upon nanoparticle labeling, comparisons to other nanoparticle-based DNA assays may be of value. Accurate comparison of detection limits is difficult and potentially controversial for a number of reasons including differing experimental conditions and the differing ways in which the limits themselves are defined. Clearly, however, the limits for the grating technique are competitive with those of initial reports on aggregation-based colorimetric detection in solution[3] but poorer than those based on surface binding and subsequent chemical amplification.[5,28,29] Perhaps conceptually most interesting are comparisons with surface plasmon resonance (SPR), since this technique, like the grating

technique, is based upon changes in refractive index. Especially pertinent are SPR reports describing colloidal gold enhancement of biomolecule binding/hybridization.[30,31] Again, in recognition of the difficulty in achieving "apples-to-apples" comparisons, it would appear that the grating approach offers a sensitivity advantage over these reports.[31] At the same time, the absolute sensitivity of commercial SPR instruments to changes in n (ca. 10^{-5} refractive index units), determined by shifts in critical angle, exceeds by about 10-fold the absolute sensitivity of the grating technique, determined by changes in diffraction efficiency, at least at this stage in the grating measurement technique's development.

Finally, the multicolor diffraction measurements and the color-selective nature of the observed resonance amplification point toward multiplexing methodologies. The multicolor experiment described here reports on the aggregation state of a homogeneous nanoparticle probe that is complementary to a single target strand, while also engendering a novel single-step/single-solution method for ssDNA detection. By using multiple, uniquely labeled nanoparticle probes of varying size, shape, or composition encoding for different target strands, multicolor diffraction-based detection should be able to simultaneously discriminate and identify an unknown target. Analogous multicolor SPR experiments[32] should ultimately display similar attributes.

Conclusions

The combination of chemoresponsive grating-based diffraction modulation and nanoparticle labeling comprises a promising new approach to ssDNA detection. Binding of target DNA strands to a complementary DNA derivatized micropattern (grating) alters the refractive index contrast of the grating and yields easily measured changes in diffraction efficiency. Utilization of a nanoparticle probe, heavily functionalized with ssDNA complementary to the target DNA, results in significant signal amplification. The basis for the amplification is the plasmon absorption of the anchored nanoparticles, proximal to the grating structure, which induce a modulation in the local refractive index contrast, according to the Kramers−Kronig transformation. The degree of resonance of the diffraction probe beam with the plasmon absorption largely defines the probe wavelength dependence of the amplification, which can be either positive or negative. When nanoparticles are employed as hybridization beacons, these nonoptimized, first-generation devices display detection limits competitive with molecular fluorescence approaches[4] for the real-time hybridization of target ssDNA, while showing increased sequence specificity, which derives from the cooperative binding and melting properties of nanoparticle probes.[7] The successful modeling of multicolor responses points to the intriguing possibility of target multiplexing by simultaneous utilization of multiple shapes, sizes, and/or

(28) Taton, T. A.; Mirkin, C. A.; Letsinger, R. L. *Science* **2000**, *289*, 1757−1760.
(29) Cao, Y. W. C.; Jin, R.; Mirkin, C. A. *Science* **2002**, *297*, 3820−3821.
(30) Lyon, L. A.; Musick, M. D.; Natan, M. J. *Anal. Chem.* **1998**, *70*, 5177−5183.
(31) He, L.; Musick, M. D.; Nicewarner, S. R.; Salinas, F. G.; Benkovic, S. J.; Natan, M. J.; Keating, C. D. *J. Am. Chem. Soc.* **2000**, *122*, 9071−9077.
(32) Recently a two-wavelength SPR experiment has been reported, though not utilizing probe label absorptions for signal magnitude enhancement purposes: Zacher, T.; Wischerhoff, E. *Langmuir* **2002**, *18*, 1748−1759.

compositions of nanoparticle tags, each possessing unique optical properties.